Marine Geology xxx (2013) xxx–xxx

Contents lists available at ScienceDirect

Marine Geology

journal homepage: www.elsevier.com/locate/margeo

Erosional features as indicators of thrust fault activity (Nankai Trough, Japan)☆

Tiago M. Alves [a,*], M. Strasser [b], G.F. Moore [c]

[a] 3D Seismic Lab, School of Earth and Ocean Sciences, Cardiff University, Main Building, Park Place, CF10 3AT Cardiff, United Kingdom
[b] Geological Institute, ETH Zurich, NO G 46, Sonneggstrasse 5, 8092 Zurich, Switzerland
[c] Department of Geology & Geophysics, University of Hawaii, 1680 East–West Rd., POST 813 Honolulu, HI 96822, USA

ARTICLE INFO

Article history:
Received 25 March 2013
Received in revised form 11 July 2013
Accepted 17 July 2013
Available online xxxx

Keywords:
Continental margin
Accretionary wedge
Sediment taper
Erosion
Tectonic uplift
Seafloor deformation

ABSTRACT

A submarine channel system and basal ramps of a Quaternary mass-transport deposit (MTD) are shown to represent thrust fault activity in the Nankai accretionary wedge. Variations in channel bed slope, height and width of submarine channels and gullies indicate uplift and sediment bypass seaward from a margin-dominating out-of-sequence thrust, the megasplay fault (MSF), at <1.67–1.46 Ma. Between ~1.05 and 0.85 Ma, a younger mass-transport deposit (MTD 6) was detached at different depths. Demonstrating the significant deformation observed in the study area, the direction of transport of MTD 6 differs 30°–45° from the strike of scarps and ramps at its base, which are parallel to the structural contours of thrust anticlines underneath. This character contrasts to the geometries frequently documented in frontally-emergent submarine landslides. Oblique basal ramps form significant boundaries between zones of MTD 6 with distinct acoustic and, suggestively, petrophysical properties. As a result of this study, we postulate that developed channel systems can erode the upper continental slope and lead to bypass of substantial volumes of sediment to distal parts of accretionary wedges. This process bears the potential of generating periods of more intense thrust-wedge deformation than those predicted by mathematical and physical models based on present-day taper geometries. On a regional scale, the observations in this paper are important as they indicate a more diffuse distribution of deformation in the Nankai accretionary wedge than previously assumed for the MSF region.

1. Introduction

The mechanics behind the deformation of accretionary wedges have been described by the Coulomb wedge theory, in which the outer wedge is considered at a critical state (i.e. the wedge is on the verge of failure) or reaching critical state after large earthquakes (Davis et al., 1983; Dahlen, 1984, 1990; Wang and Hu, 2006). In these conditions, rapid mass redistribution can occur throughout, or across, large regions of accretionary wedges (Beaumont et al., 1999; Dominguez et al., 2000; von Huene et al., 2005; Camerlenghi and Pini, 2009; Smit et al., 2010; Yamada et al., 2010, 2012). Yet, few examples of erosional features with impact on accretionary wedge geometry and growth have been documented (Berger and Johnson, 1980; Davis et al., 1983; Konstantinovskaya and Malavieille, 2005; Graveleau and Dominguez, 2008; Konstantinovskaya and Malavieille, 2011; Buiter, 2012; Kitamura and Yamamoto, 2012). This under-representation in the literature poses important limitations, as erosional features formed adjacently to active structures can be helpful markers of tectonic deformation on convergent margins (Bangs and Cande, 1997; Dominguez et al., 1998; Tsuru et al., 2000; Tamaki et al., 2009). In particular, to recognise enhanced periods of tectonic deformation on convergent margins is important because they are associated with: a) a relative increase in the activity of large-scale seismogenic faults; b) the generation of major fluid-flow paths extending from subducted slabs to the surface, and; c) the triggering of recurrent slope instability events (Lucente and Pini, 2008; Kitamura and Yamamoto, 2012; Ratzov et al., 2012).

Mass-transport deposits (MTDs) are primary features capable of imposing changes to the architecture of accretionary wedges (Ashi and Taira, 1992; Wang and He, 1999; Buiter, 2012). In such deposits, basal erosional features can be important to the recognition of tectonically active structures, similar to what is documented for sub-aerial landslides (Masek et al, 1994; Matsushi et al., 2006; Korup et al., 2007; Lavé and Avouac, 2011). A key character in basal erosional features of MTDs is that they resemble brittle structures (Gee et al., 2005; Ashabranner et al., 2010). Brittle structures reflect the loss of internal cohesion along specific surfaces when the elastic limit is exceeded under an applied stress (Hancock, 1985; Sibson, 1998).

* Corresponding author. Tel.: +44 2920876754.
E-mail address: alvest@cardiff.ac.uk (T.M. Alves).

0025-3227/$ – see front matter © 2013 The Authors. Published by Elsevier B.V. All rights reserved.
http://dx.doi.org/10.1016/j.margeo.2013.07.011

A second example of features with impact on the evolution of accretionary wedges comprises submarine channels generated during periods of enhanced tectonic uplift. On land, there are established scale-relationships between the rates of tectonic uplift and the evolution of specific landscape features (Mann et al., 1998; Humphrey and Konrad, 2000; Maruyama and Lin, 2000; Nakada et al., 2002; Finnegan et al., 2005; Matsushi et al., 2006; Kagohara et al., 2009). Similar relationships have been established for submarine channels, particularly in upper slope areas where downslope eroding sediment flows are known to promote headward erosion (Pratson et al., 1994; Pratson and Coakley, 1996; Mitchell, 2005). Incision rates of channels are generally assumed to be a function of their geometry, with the landscape evolving towards a steady state in which the lowering of topography by erosion is equal to uplift (Lague et al., 2003; Huyghe et al., 2004; Turowski et al., 2006; Heiniö and Davies, 2007; Turowski et al., 2008, 2009; Covault et al., 2011). As a result, three main parameters vary consistently in submarine channels, gullies and furrows as they do in their onshore counterparts: (1) channel/gully bed slope gradient increases with increasing tectonic uplift of the substrate, demonstrating a close relationship between erosion and seafloor deformation; (2) drainage basins with complex channel networks (orders 2–3) are installed after an initial phase showing relatively low rates of incision; (3) the width of erosional features decreases and the depth of incision increases proportionally to tectonic uplift (Orange, 1999; Mitchell, 2005; Turowski et al., 2006; Kolla, 2007; Covault et al., 2011; Turowski et al., 2008). Moreover, tectonic uplift on continental margins is frequently associated with seafloor faulting and gully erosion atop active anticlines (e.g. Mountjoy et al., 2009), a process further emphasised by climatic and oceanographic phenomena (Lewis et al., 1994; Micallef and Mountjoy, 2011).

This paper explores a section of the tectonically active Nankai accretionary wedge offshore Japan to elucidate the importance of erosional features as proxies to recognise the margin's tectono-morphological development (Fig. 1). This approach led us to postulate that enhanced periods of erosion, as the incision of submarine channel systems, affected the balance of the critical taper offshore Nankai after 1.67 Ma. This imbalance precluded the onset of a feedback loop favouring further fault propagation, seismic activity and slope instability as a part of a process that ultimately resulted in the deposition of a Quaternary mass-transport deposit (MTD 6, Expedition 333 Scientists, 2011).

The timings and rates of uplift of structures offshore Nankai are here related to the evolution of submarine channel systems and basal scarps of MTDs. This is achieved by compiling morphological data such as width, height and orientation of seafloor erosional features. For this purpose, we use 3D seismic and borehole data to analyse the progressive incision of submarine channels adjacently to thrust faults (named S1 and S2 in this paper), and associated anticlines (A1 to A5) located downslope from a large out-of sequence thrust, the megasplay fault (MSF, Expedition 333 Scientists, 2011) (Figs. 2 and 3). Later in this paper a Quaternary MTD is investigated (MTD 6, Expedition 333 Scientists, 2011), the source area of which has been interpreted to coincide with the active MSF zone (Strasser et al., 2011) (Fig. 2a).

In summary, the scientific objectives of this paper are:

- To document the incision of a channel system over uplifting thrust anticlines located downslope from the MSF;
- To investigate how the geometry of ramps and flats below a Quaternary MTD relates to active thrust faults and associated anticlines;
- To understand why basal ramps mark zones of MTDs with distinct internal seismic characters;
- To assess statistical parameters associated with the progressive development of the studied channel system, and how these relate to seafloor uplift, splay fault activity and, ultimately, to the stability of critical tapers of convergent margins.

This work concludes on the progressive development of erosional features on the Nankai slope between 1.67 and 0.85 Ma, and their use as proxies for the recognition of active fault structures in accretionary wedges.

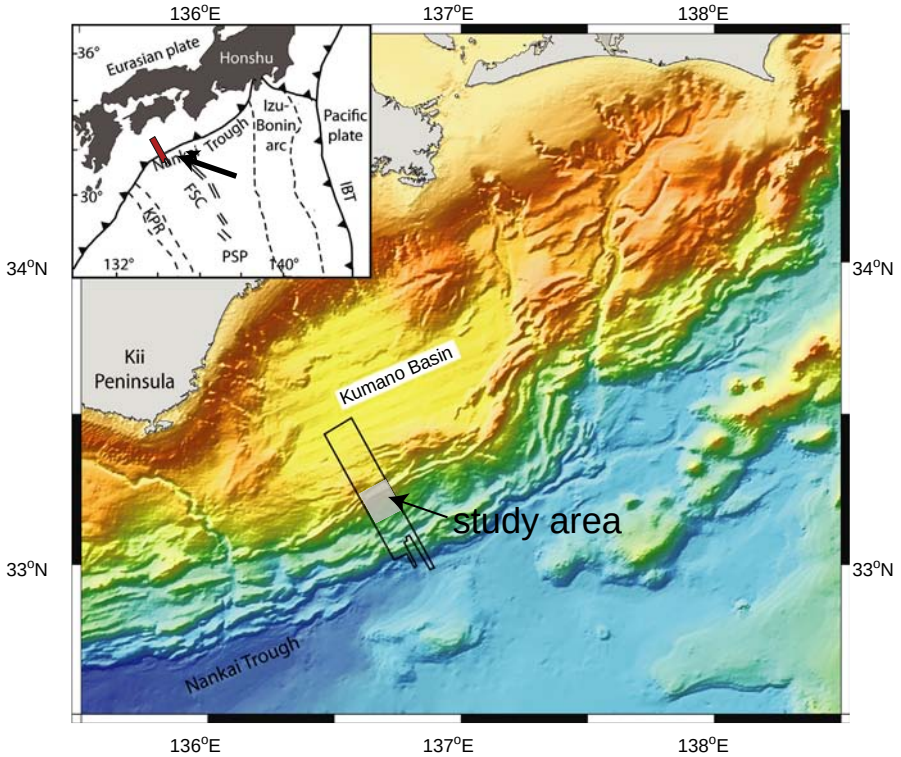

Fig. 1. Location of the study area and Kumano Transect across the Nankai Trough accretionary wedge. Arrow in inset indicates the position of the interpreted 3D seismic volume in SE Japan. IBT-Izu-Bonin Trench; KRP-Kyushu-Palau Ridge; FSC-Fossil Spreading Centre; PSP-Philippine Sea Plate.

Please cite this article as: Alves, T.M., et al., Erosional features as indicators of thrust fault activity (Nankai Trough, Japan), Marine Geology (2013), http://dx.doi.org/10.1016/j.margeo.2013.07.011

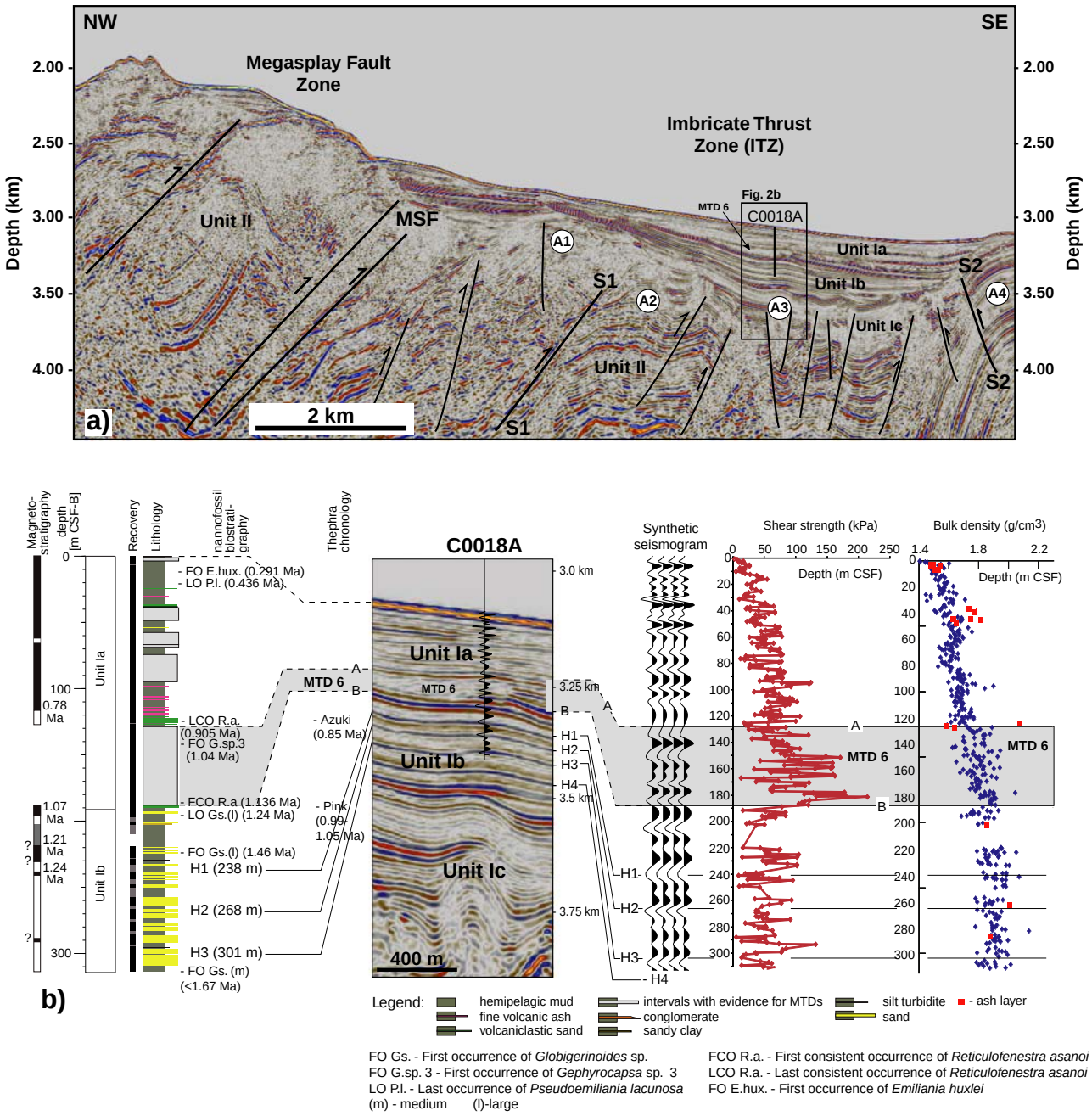

Fig. 2. (a) Depth-migrated seismic profile (inline 2315) across the Nankai continental slope showing the location of structural zones, thrust faults S1 and S2 and thrust anticlines A1 to A4 referred to in the text (Moore et al., 2007). The location of the interpreted 3D seismic block and IODP Hole C0018A is shown in Fig. 3. (b) Sedimentary log of Hole C0018A tying the interpreted horizons H1 to H4, A, B, to stratigraphic, synthetic seismic, shear strength and bulk density data. Above the interpreted channel system is a mass-transport deposit drilled during IODP Expedition 333 (MTD 6, Expedition 333 Scientists, 2011).

2. Data and methodology

A three-dimensional (3D) pre-stack depth migrated (PSDM) seismic volume covering part of the Nankai Trough accretionary wedge was interpreted in this work (Fig. 1). We selected a sub-volume in water depths ranging from 1750 m to 3200 m (Figs. 2a and 3). This sub-volume has an inline spacing of 12.5 m, for a crossline spacing of 18.75 m, and was acquired with a 2-source array with four receiver cables spaced 150 m apart. Each receiver cable was 4500 m long with 360 receiver groups at 12.5 m spacing, and acquired nominal 60-fold data. Data processing included pre-stack multiple removal and data conditioning (e.g., amplitude recovery, time-variant filtering, and predictive deconvolution) followed by 3D pre-stack depth migration (Moore et al., 2009). Seismic resolution approaches 6 m at the depth range of erosional features in this paper, based on the dominant wavelength of ~24 m observed on synthetic logs and seismic profiles (Fig. 2).

A series of seismic horizons were interpreted below the base (horizon B) of MTD 6, which was drilled during IODP Expedition 333 (Expedition 333 Scientists, 2011) (Fig. 2). From the interpreted horizons, five were chosen for structural mapping (horizons B, and H1 to H4; Figs. 2b, 4 and 5). Specifically, horizons B, H1 and H3 were correlated with nannofossil dates obtained during Expedition 333 through the use of synthetic seismic data. These synthetic data were computed using Moisture And Density (MAD) bulk density data, and p-wave velocity (V_p) measurements obtained onboard (Expedition 333 Scientists, 2011). We then extracted a series of

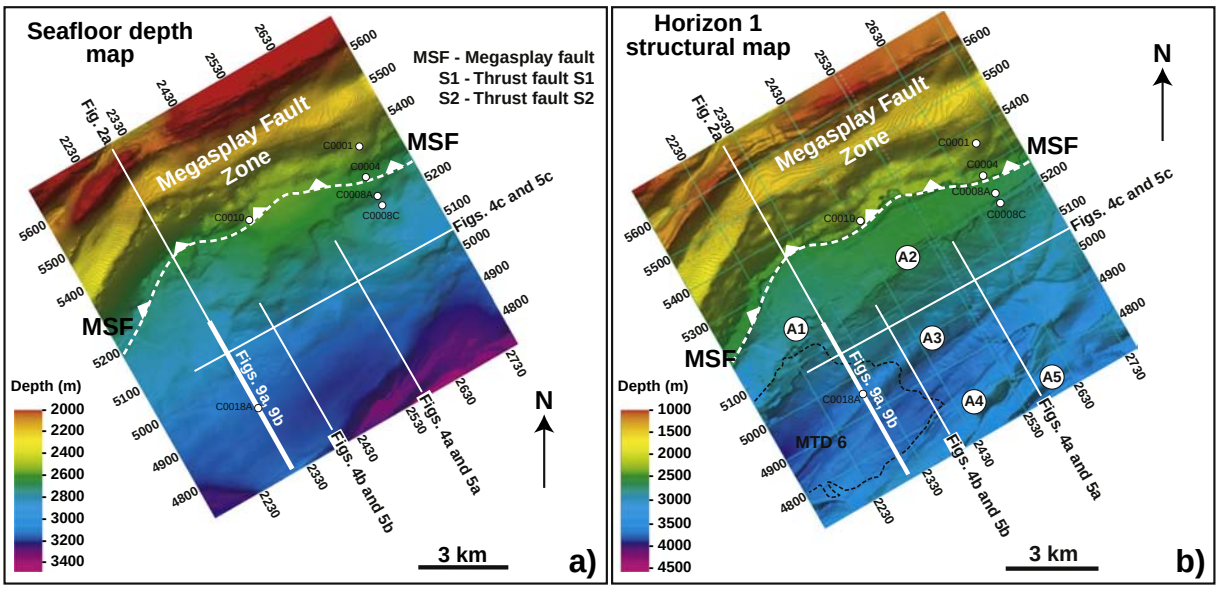

Fig. 3. (a) Seafloor map showing the location of main structural features in the study area, IODP sites and the extent of the interpreted seismic volume. (b) Structural map of horizon H1, the first continuous, negative-polarity basal reflection not truncated by MTD 6. A1 to A5 denote thrust anticlines associated with main thrust faults.

parameters from observed submarine channels and gullies in horizons H1 to H3, including: (1) channel bed slope, (2) channel width, and (3) channel height, a proxy for the erosional power of gullies and channels (Figs. 5 and 6).

Submarine channels and gullies were divided in fifteen (15) different segments, and profile data were collected across their axes (Fig. 7). Average values for channel bed slope, channel height and channel width were acquired in each of the 15 segments (Fig. 8 and Table 1). Segment 1 represents the southernmost portion of transverse channels A to J, upslope from the axial channel, while Segment 15 refers to their northernmost segments (Fig. 6). The values obtained were also discriminated for channels A to C, D to F and G to J to highlight along strike (E to W) variations in morphometric parameters (Fig. 8 and Table 1).

The seismic resolution and standard error involved in the collection of statistical data were considered when plotting channel width and heights. In this paper, the standard error comprises the standard deviation of the sampling distribution of channel widths and heights.

3. Geological setting

3.1. Structure and physiography of the Nankai accretionary wedge

The Nankai accretionary complex results from subduction of the Philippine Sea plate beneath the Eurasian plate along the Nankai Trough (Fig. 1). The study area is located at the upper, landward part of the imbricate thrust zone (ITZ) along the Kumano transect, offshore SE Japan (Moore et al., 2009) (Figs. 1 and 2). Between the ITZ and the Kumano Basin is observed a regional Megasplay Fault (MSF) (Park et al., 2002; Tobin and Kinoshita, 2006). The shallow part of this MSF consists of a complex thrust system with upslope breaking branches (Fig. 2a). These branches dissect the ITZ and override younger slope basin sediments (Moore et al., 2007) as in the case of the S1 and S2 thrusts (Fig. 2a). The S1 and S2 thrusts are associated with prominent thrust anticlines (A1 to A5) and reflect diffuse deformation on the upper continental slope in response to movement of the out-of-sequence MFS (Figs. 2a and 3b). Thus, both the studied submarine channel system and the mass-transport deposit (MTD 6, Expedition 333 Scientists, 2011) were generated in what is interpreted in this work as a broad zone of deformation within the ITZ (Figs. 2 and 3).

Seafloor deformation in the ITZ is marked by ENE-trending anticlines in the east and by a southward dipping monocline to the west (Kimura et al., 2011; their Fig. 11a and b). In this same region, the uppermost sediments of the accretionary prism are cut by NW- to NNW-trending faults (Fig. 3b). Kimura et al. (2011) interpreted these as comprising oblique-slip normal faults, consistent with the present-day stress field inferred from borehole breakouts, fractures in cores, and anelastic strain recovery of the cores (see also Byrne et al., 2009). These faults are mostly confined to the uppermost strata in the accretionary prism, denoting a decoupling in stresses between the first ~1250 m of strata and units below, in which compression predominates (Lin et al., 2010).

Previous studies indicate that the present-day tectonic and depositional settings of the study area started at ~2.2 Ma in a frontal wedge-toe position (Strasser et al., 2009). Splay fault movement was initiated at ~1.95 Ma in the lower part of the accretionary wedge. Ongoing megasplay slip occurred since ~1.55 Ma (Strasser et al., 2009). Towards its eastern part displacement ceased at ~1.24 Ma, suggesting that it only experienced a relatively short period of high activity between ~1.55 and 1.24 Ma. In addition, Gulick et al. (2010) recognised a major phase of landward tilting in the Kumano Basin, landward of the MSF, and inferred activity of the MSF system between 1.3 and 1.0 Ma. This phase postdates an earlier phase of asymmetric forearc-high uplift, with strongest uplift in the southwestern part of the Kumano transect occurring together with splay fault steepening and underthrusting of large volumes of sediment (Bangs et al., 2009).

3.2. Significance of recurrent slope instability through the Pliocene–Quaternary

Ages for MTDs in the study area range from 2.87 Ma to Recent (<100 years b.p.) (Kimura et al., 2011; Strasser et al., 2011, 2012). The largest MTD 6 covers more than 20 km^2 and has a maximum thickness of ~182 m (Strasser et al., 2011). MTD 6 has been drilled and cored at a location where it reaches a thickness of 61.5 m (MTD 6, Expedition 333 Scientists, 2011). It is dated based on nannofossil specimens and considered to have been emplaced between 0.85 and 1.05 Ma (Strasser et al., 2012).

Seismic data from the study area reveal a complex interaction between fault propagation folding, seafloor instability, and faulting (Kimura et al., 2011). Mass-transport deposits were documented around the MSF by Kimura et al. (2011) and Strasser et al. (2011).

Please cite this article as: Alves, T.M., et al., Erosional features as indicators of thrust fault activity (Nankai Trough, Japan), Marine Geology (2013), http://dx.doi.org/10.1016/j.margeo.2013.07.011

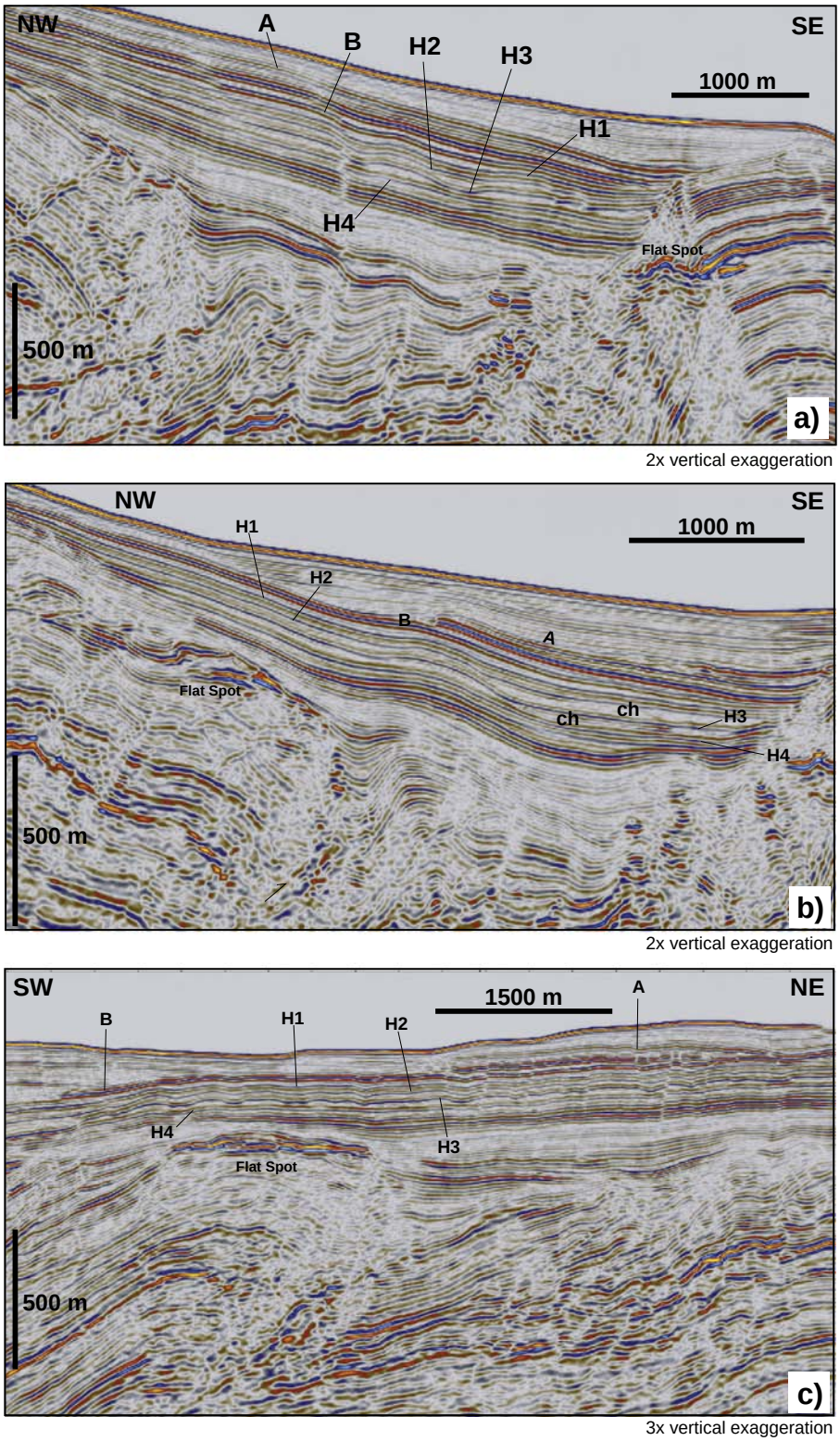

Fig. 4. (a) Depth-migrated seismic profile (inline 2533) showing the investigated submarine gullies and the relative position of horizons H1 to H4, A and B. (b) Depth-migrated seismic profile (inline 2389) transverse to the larger part of the axial submarine channel in the study area (ch), and highlighting its size and relative location in the Imbricate Thrust Zone (ITZ). (c) Depth-migrated seismic profile (crossline 5050) illustrating the presence buried thrust anticlines underneath horizons H1 to H4. The location of the seismic sections is shown in Fig. 3.

Kimura et al. (2011) suggested these mass movements to be related to slip along the MSF, with seafloor sediment becoming oversteepened and/or shaken by periodic earthquakes. Direct influence of splay fault activity was, however, likely reduced across MTD 6 as no direct evidence for displacement younger than ~1.24–1.0 Ma is observed along the seaward branch of the MSF (Kimura et al., 2011). Taking into consideration that reduced differential compaction occurred in slope strata overthrusted by the hanging-wall portion of the MSF, and that related lateral transmission of fluids was likely reduced after ~1.24–1.0 Ma, Strasser et al. (2011) considered this relative absence of MSF movement

Please cite this article as: Alves, T.M., et al., Erosional features as indicators of thrust fault activity (Nankai Trough, Japan), Marine Geology (2013), http://dx.doi.org/10.1016/j.margeo.2013.07.011

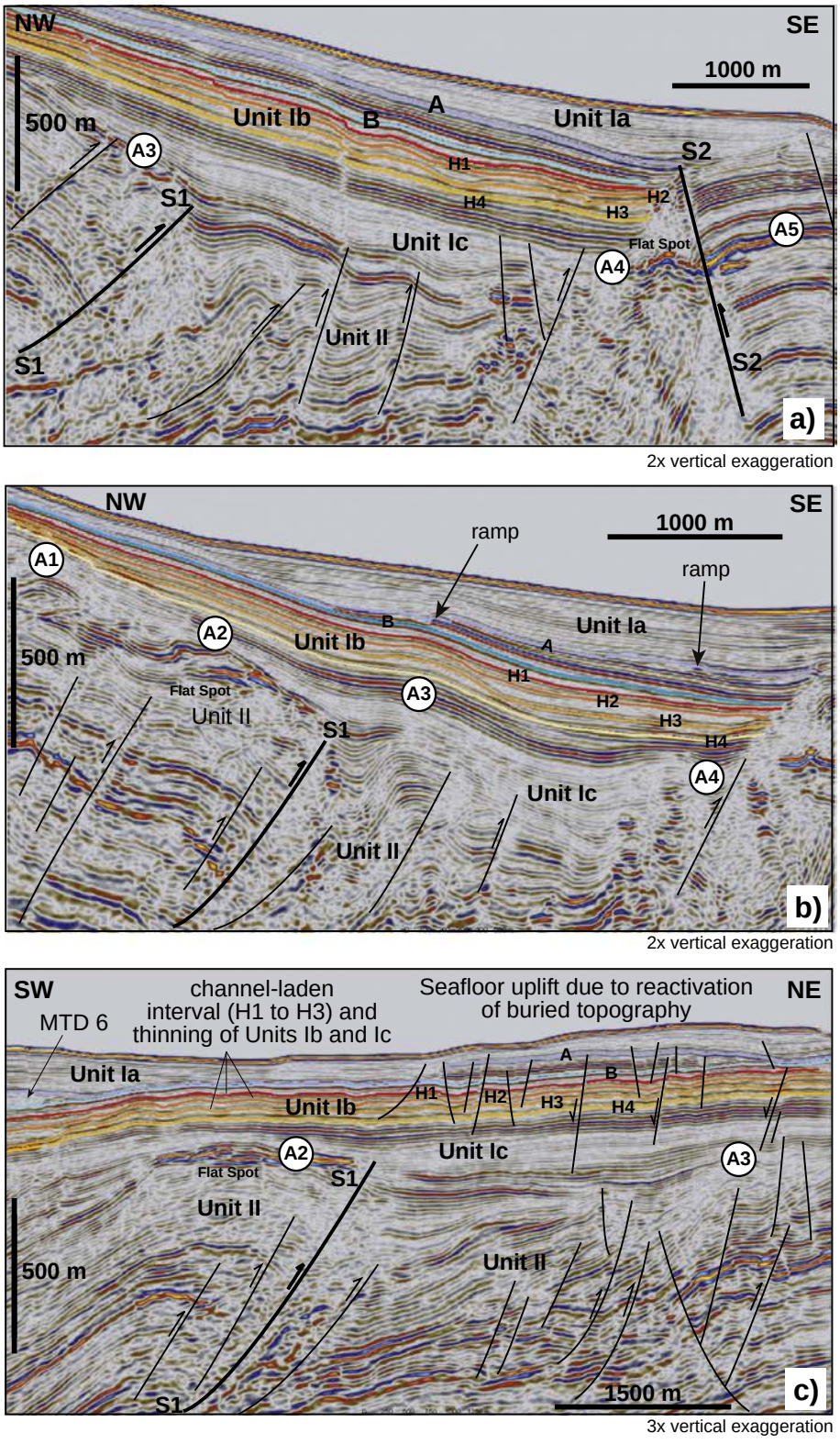

Fig. 5. Interpreted depth-migrated seismic profiles in Fig. 4. Main thrust anticlines A1 to A5 are shown. (a) Inline 2533 showing the submarine channel system between H1 and H4 and the structural complexity of thrusts in Unit II. (b) Inline 2389 highlights the morphology of the axial channel developed between S1 and S2. (c) Crossline 5050 highlights the position of large thrust anticlines (A2 and A3) underneath MTD 6 and the region of channel incision. Low angle thrusts and adjacent folded depocentres are shown in the seismic sections within Unit II. The location of the seismic sections is shown in Fig. 3.

as a plausible explanation as to why younger MTDs in the study area are smaller than their older counterparts. Significant ground accelerations recorded during large earthquakes, and related transient pore-pressure phenomena, constitute plausible trigger mechanisms for sediment instability in the MSF area (Ikari et al., 2011). This idea is supported by core-derived evidence for the most recent mobilization and redeposition of sediment; a thin mud-brecciation layer related to the 1944 Mw 8.2 Tonakai earthquake (Sakagushi et al., 2011).

Frequent mass-wasting and syn-sedimentary deformation in the study area may therefore be related to the fact that deformation is not

Please cite this article as: Alves, T.M., et al., Erosional features as indicators of thrust fault activity (Nankai Trough, Japan), Marine Geology (2013), http://dx.doi.org/10.1016/j.margeo.2013.07.011

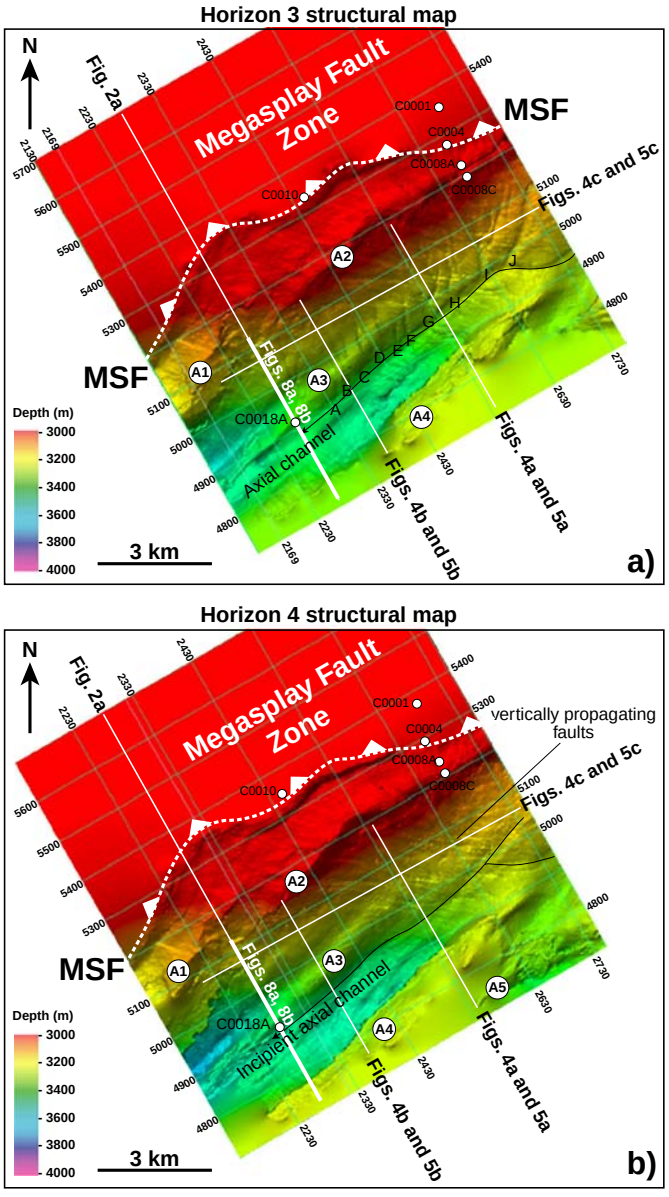

Fig. 6. (a) Structural map of horizon H3, marking the incision of the interpreted channel systems. (b) Structural map of horizon H4, preceding the incision of the channel systems in this paper. The presence of channels A to J is only observed above H4 until H1. Horizon B shows once more no evidence of erosion.

limited to the MSF itself, pointing to a structural separation between the eastern and western portions of the MSF (Kimura et al., 2011). In fact, slope deformation is proven in this work to be much broader and scattered south of the MSF, being also related to the deformation of the underlying accretionary prism.

4. Seismic stratigraphy

Seismic stratigraphic units in the study area are depicted and correlated with borehole data from IODP Hole C0018A in Fig. 2b (Expedition 333 Scientists, 2011). Based on previous information from IODP Holes C0004A, C0008A and C0008B (Expedition 316 Scientists, 2009a), the two main seismic units in the study area comprise slope sediments (Unit I) and the underlying accretionary prism (Unit II). Within Unit I, the larger MTD 6 divides the slope sediments into two distinct sub-units; one with a sandy turbidite sequence below (Unit Ib), and one with ash-bearing hemipelagites and MTDs above (Unit Ia) (Fig. 2).

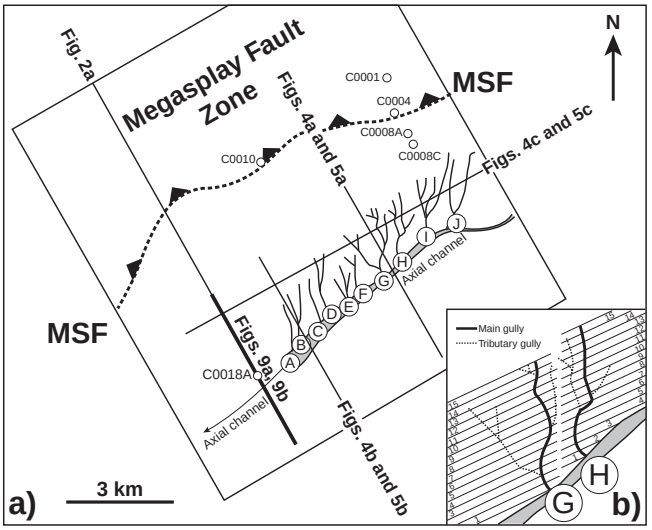

Fig. 7. Diagram showing the method used for the acquisition of morphological data in submarine channels and gullies. (a) Shows the relative position of submarine gullies in the study area, based on the map in Fig. 6a. The inset in b) illustrates the sub-division of observed channels and gullies in 15 segments, from South to North, with their average channel height, width and bed slope measured accordingly. A to J — Submarine channels and gullies interpreted in this study.

4.1. Unit I: Slope basin succession, latest Pliocene–Holocene

Unit I comprises strata younger than ~1.46–1.77 Ma and 1.95–2.4 Ma, overlying accreted MTDs (2.06–2.52 Ma) and trench turbidites (2.4 Ma) at Sites C0004 and C0008 (Kimura et al., 2011). Three sub-units are recognised in the study area.

4.1.1. Unit Ia

Unit Ia comprises silty mud and silty turbidites with several ash layers (Kimura et al., 2011). These strata are imaged as low-amplitude reflections of poor to moderate continuity denoting erosion by MTDs (Figs. 2a and 4). At Site C0018A, ash layers and six intervals with evidence of MTDs (Fig. 2b) are observed. The base of Unit Ia coincides with MTD 6, which was dated to have been emplaced between ~0.85 and 1.05 Ma (Strasser et al., 2012) (Fig. 2b).

4.1.2. Unit Ib

At Site C0018, Unit Ib comprises coarse turbidite and ash layers, with interbedded silty mud and mud. The unit is seen as a succession of continuous high-amplitude reflections (Figs. 2a and 4). Nannofossils and magnetostratigraphy show that the age of Unit Ib ranges from 1.55 to 1.24–1.0 Ma at Sites C0004A and C0008A,B (Expedition 316 Scientists, 2009a,b; Strasser et al., 2009, 2012). At Site C0018A, the oldest sediments drilled are younger than 1.67 Ma, but the base of the unit has not been reached (Fig. 2b).

4.1.3. Unit Ic

At Sites C0008A and C0008C, Unit Ic consists of greenish/grey silty clay with beds of sand, sandy silt, silt, and volcanic ash layers (Expedition 316 Scientists, 2009a). The unconformity between the underlying prism strata and MTDs at the base of Unit I occurs between 1.95 and 2.4 Ma according to nannofossil chronology and magnetostratigraphy (Kinoshita et al., 2009; Strasser et al., 2009). On seismic data, Unit Ic is shown as a low- to moderate-amplitude unit showing significant folding and faulting (Figs. 2a and 4).

4.2. Unit II: Accretionary prism: Pliocene and older

In Hole C0004A, Unit II comprises accreted Pliocene hemipelagic mud and ash layers, the latter of which are more prominent in the

Please cite this article as: Alves, T.M., et al., Erosional features as indicators of thrust fault activity (Nankai Trough, Japan), Marine Geology (2013), http://dx.doi.org/10.1016/j.margeo.2013.07.011

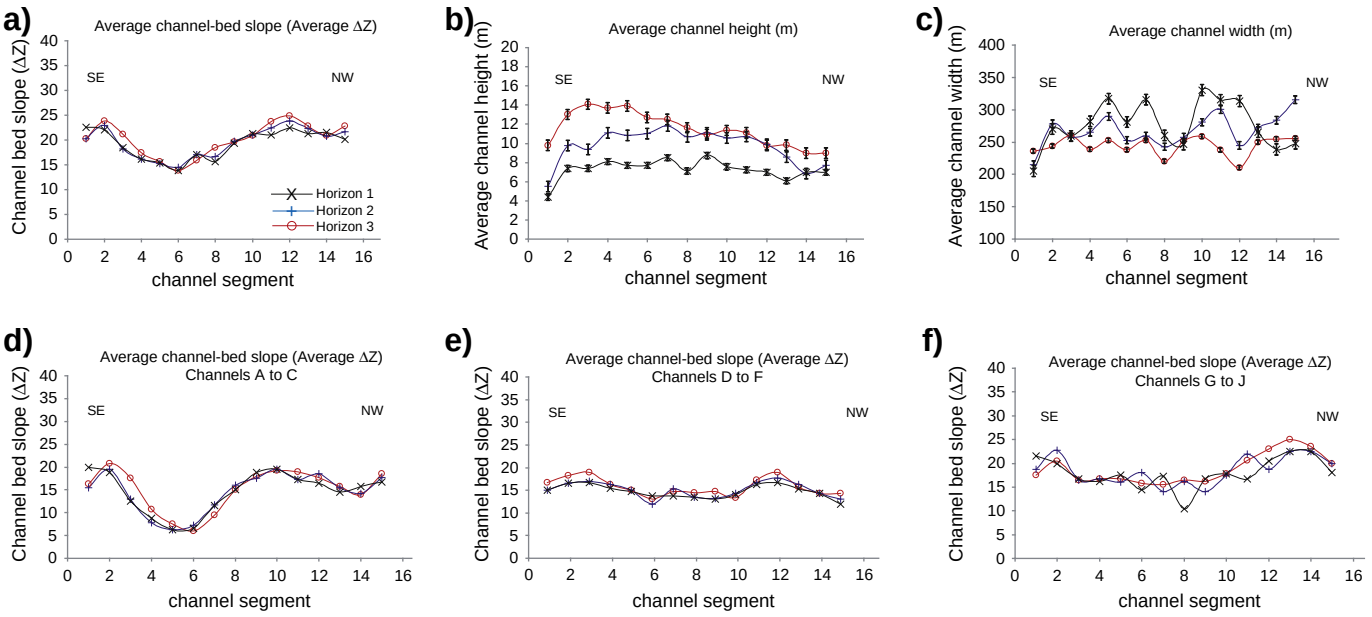

Fig. 8. Graphs depicting statistical data for channels A to J. (a) Average channel bed slope (b) Average channel width. (c) Average channel height. (d) Average channel bed slope for channels A to C. (e) Average channel bed slope for channels D to F. (f) Average channel bed slope for channels G to J. Error bars indicate the standard error of measured values.

lower part of the splay fault zone (Expedition 316 Scientists, 2009b; Kimura et al., 2011). On seismic data, high-amplitude strata showing significant folding and faulting are observed at the core of the accretionary complex. Expedition 314 (Expedition 314 Scientists, 2009) drilled mudstones in Unit II equivalent to lower Shikoku Basin deposits (e.g. Ike et al., 2008).

5. Submarine channels and gullies on the upper slope

5.1. Morphology and age constraints on channel incision

Three horizons were selected (horizons H1 to H3) to illustrate the evolution of an interpreted channel system incising the slope between the S1 and S2 faults (Figs. 2 and 4). Below H3, and above H1, the imaged strata show no further evidence for channel incision on the continental slope (Figs. 4 and 5). Corroborating this interpretation, a NE–SW axial channel is observed across the continental slope above horizon H4, fed by transverse submarine channels and gullies (Figs. 4b, 6 and 7). The height of this axial channel is substantially reduced above horizon H2 (Figs. 4b). In parallel, the interpreted data indicate a rapid incision of the submarine channels and gullies above horizon H4, with their progressive abandonment and filling occurring towards the bottom of MTD 6 (horizon B, Figs. 5b and 8b).

Nannofossil specimens at Site C0018 indicate horizon H1 to be older than the first occurrence of large *Gephyrocapsa* spp. (>5.5 μm) at ~1.46 Ma (Fig. 2b). In turn, *Gephyrocapsa* spp. medium was recovered in the core catcher of the last section drilled, 11 m below Horizon 3 (Expedition 333 Scientists, 2011), indicating it is younger than 1.67 Ma. Horizon H2 lies in between these two intervals (Fig. 2b). As a result, nannofossil data in Hole C0018A indicate a period of channel incision and contemporaneous tectonic uplift ranging from <1.67 Ma to ~1.46 Ma, ages coinciding partly with an interpreted episode of high MSF activity around ~1.55–1.24 Ma (Strasser et al., 2009), but differing from the episode of high MSF activity at 1.3–1.0 Ma inferred for the Kumano Basin (Gulick et al., 2010).

Table 1
Statistical data measured in channels A to J. The table show average values for channel bed slope, width and height in each of the interpreted channel segments, and for the entire channel system at the bottom.

	Channel bed slope (m)			Channel width (m)			Channel height (m)		
Segment	H3	H2	H1	H3	H2	H1	H3	H2	H1
1	20	20	23	235	215	205	10	6	4
2	24	23	22	244	278	270	13	10	7
3	21	18	18	261	258	260	14	9	7
4	18	16	16	239	265	282	14	11	8
5	16	15	15	252	290	318	14	11	8
6	14	15	14	238	252	281	13	11	8
7	16	17	17	253	260	315	13	12	9
8	18	17	16	220	243	261	12	11	7
9	20	20	19	252	258	247	11	11	9
10	21	21	21	258	281	330	11	11	8
11	24	23	21	238	301	315	11	11	7
12	25	24	22	210	245	313	10	10	7
13	23	22	21	250	272	266	10	9	6
14	21	21	22	254	284	239	9	7	7
15	23	22	20	255	315	248	9	8	7
Average	20	20	19	244	268	277	11	10	7

5.2. Statistical analysis of channels and gullies

In order to relate erosion in the study area to local tectonic uplift we used geomorphology concepts in Lague et al. (2003) and Turowski et al. (2009) to compute the series of graphs in Fig. 8. Slope gradients, height and width were measured for the 10 observed channels/gullies in horizons H1 to H3 (Figs. 5 and 6a). The data in Fig. 8 and Table 1 confirm that average channel bed slope values show minor variations through horizons H1 to H3 (Fig. 8a). This character is accompanied by a marked undulating bed profile towards the western part of the study area (A to C) (Fig. 8d). In contrast, D to F have regular bed slope profiles, while G to J show larger slope gradients close to the S1 thrust fault and associated A2 anticine (Fig. 8e and f).

The interpretation of morphometric data generally suggests post-incision tectonic deformation to predominate in the areas where channel bed slope increases, and where the resulting channel bed slope curve is markedly sigmoidal (see Lague et al., 2003; Turowski et al., 2009). In the study area, channel width increases gradually from horizons H3 to H1, and channel height is also reduced above H2, above which it approaches the resolution limit of the interpreted seismic volume (Fig. 8b and c). This pattern indicates incision of

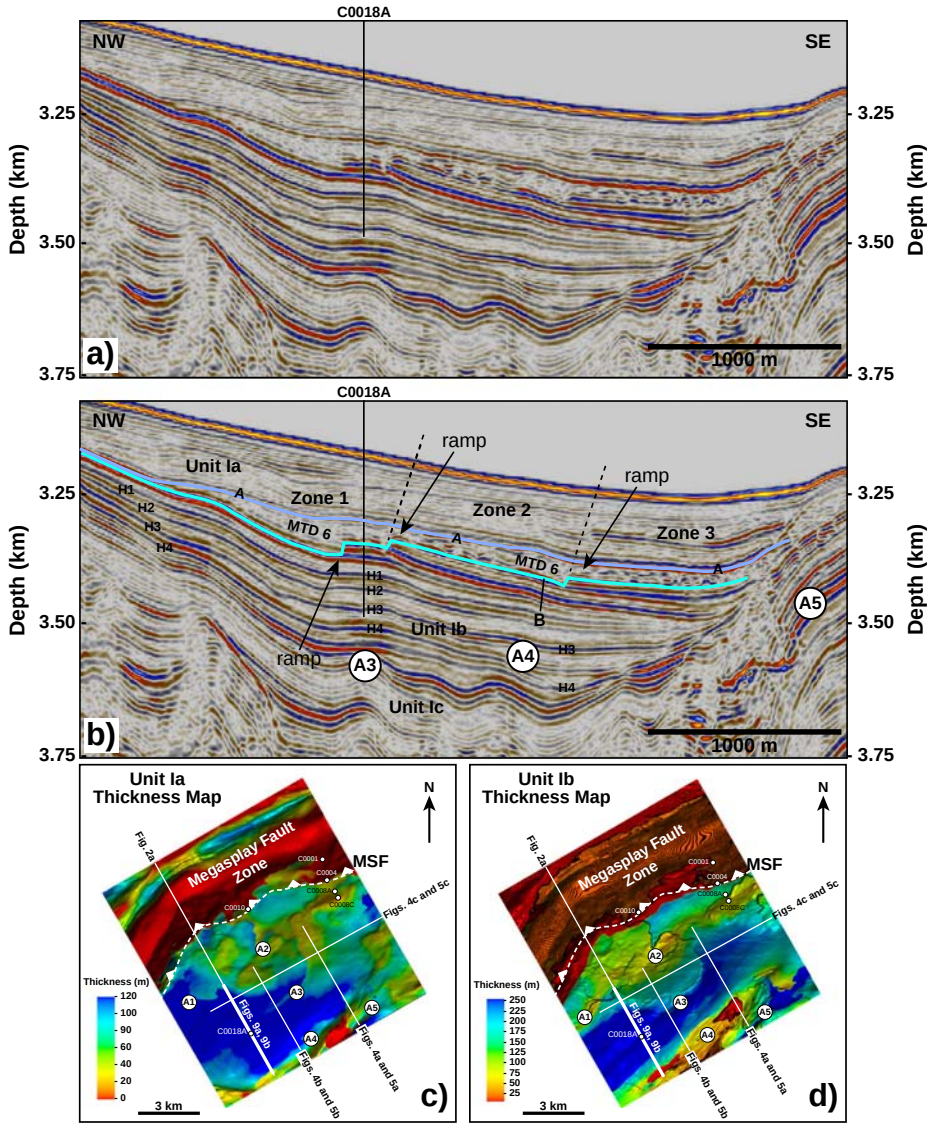

Fig. 9. (a) Depth-migrated seismic profile (inline 2315) crossing well C0018 highlighting the stratigraphic position of MTD 6 and three zones with distinct internal character in this same mass-transport deposit. The location of the seismic sections is shown in Figs. 3, 9c and 9d. (b) Interpreted seismic section in (a) highlighting the frontal ramps in horizon B and corresponding horizons mapped at the base (horizon B, in blue), and top of MTD 6 (horizon A, in purple colour). See Fig. 2b for the stratigraphic position of these same horizons. (c) Thickness maps for Unit Ib showing a reduction in its thickness above and adjacently to thrusts S1 and S2, an evidence of seafloor due to seafloor uplift and activity of these same faults. (d) Thickness map for Unit Ia, depicting the reduction in the activity of S1, contrasting with the recent uplift recorded along S2. In c) and d) thickness data were computed only for the area south of MSF. North of the MSF is depicted a seafloor structural map (1800 to 2100 m). (For interpretation of the references to colour in this figure legend, the reader is referred to the web version of this article.)

channels in horizon H3, with their progressive abandonment occurring towards horizon B. The relative increase in channel bed slope observed towards the northwest (Fig. 8a) denotes tectonic uplift of the A2 anticline and MSF after the incision of the observed channel system at the level of H3 (see also Kimura et al., 2011). This occurred together with thinning of Units Ib and Ic above the A2 and A5 thrust anticlines, i.e. adjacently to the S1 and S2 thrusts (Figs. 3b, 5 and 9).

Structural maps in Fig. 6 were combined with the statistical measurements of channel bed slope, width and height in Fig. 8 to address the distribution of erosional features in the ITZ. Together with MTD 6, the predominance of erosional features between <1.67 Ma and 0.85 Ma denotes a significant period of deformation seaward of the MSF (Figs. 3 and 6). Between horizons H2 and H4, seismic reflections are cross-cut by multiple channels and gullies on the flanks of an axial channel developing ENE–WSW. Above H2, submarine channel erosion was less pronounced but MTD 6 once more reveals widespread instability seaward of the MSF, a character denoting enhanced activity of this same fault (Strasser et al., 2011) (Fig. 3). While the erosion of submarine channels is likely related to uplift between A1 and A5 due to enhanced tectonic activity in the ITZ, we interpret the S1 thrust and the MSF to become predominant features after H1. This shift is recorded by the triggering (and latter deposition) of MTD 6, and overlying MTDs, as slope attached MTDs sensu Moscardelli and Wood (2008), sourced from the immediate footwall of the larger MSF and S1 (Figs. 3, 4 and 5). In the context of the Pleistocene-Holocene evolution of the Nankai region, such an observation suggests that deformation seaward of the MSF was in the Quaternary accommodated in a wide region of the ITZ. Therefore, S1 and S2 comprised fault splays reactivated within a larger MSF, that accommodated differential stresses across a large portion of the ITZ (Fig. 2a).

6. Significance of oblique ramps and scarps at the base of MTD 6

In order to reassess the significance of ramps as kinematic indicators and proxies for the recognition of tectonically-active structures, the identification and initial mapping of discrete MTDs in vertical seismic

sections was followed by the compilation of structural and root-mean square (RMS) amplitude maps Figs. 9, 10 and 11. These maps provide measurements of the root-mean square amplitude of a seismic wave reflected at normal incidence on an interface (Brown, 1999). Amplitudes of reflected seismic waves, positive or negative, are root-squared in RMS amplitude maps, emphasising any larger reflection events over low-amplitude background strata.

Ramp-flat structures are commonly recognised as forming perpendicular, or in a parallel direction, to sediment flow during slope failure (e.g. Bull et al., 2009). However, isochron and time-structure data shows MTD 6 direction of transport to be oblique to basal ramp-flat structures, as revealed by the presence of seven step-like 1.0 to 3.0 km long headwall scarps to the north and northwest of MTD 6 (Fig. 10). Downslope from these headwalls, scarps and ramps are shown as indentations in basal glide planes that are sub-parallel to the axes of thrust anticlines in Unit Ib (Figs. 9 and 10). Strikingly, MTD 6 was triggered as a series of proximal slabs detached at different levels (Fig. 10).

As cusp-shaped headwall scarps of landslides are aligned perpendicularly to the transport direction of the failed mass of sediment (Nemec, 1990; Hampton et al., 1996), each cusp is usually assumed to represent a translation vector, with the resulting sum of vectors for each of the headwall cusps providing an estimate of the transport direction for the entire failed mass. In the study area, scarps and frontal ramps form angles of 30–45° with what is roughly a N–S transporting direction for MTD 6 (Fig. 10). In parallel, strata below the ramps show dip angles varying 0–10° in relation to the angle of the basal glide surface (Fig. 11). This character indicates that the strike of ramps below MTD 6 is not directly related to its direction of transport, but rather to the strike of underlying structures with seafloor expression (Figs. 3 and 10). Ramps are also observed over thrust anticlines in the distal accumulation zone of MTD 6 (Fig. 10).

The generation of the observed scarps and ramps can be explained by two distinct processes: 1) considering a single landsliding event, downslope movement in MTD 6 could have been responsible for the erosion and formation of cuesta-like relief above positive seafloor features; and 2) older landsliding events may have left ramps on the seafloor, in which case MTD 6 is not directly related with the features mapped at its base. We favour the first explanation because: a) ramps are accompanied by variations in the thickness and internal character of MTD 6; b) there are no vertically-propagating faults below frontal ramps in MTD 6, excluding their generation as fault-bounded geological features, and; c) strata show varying dip angles across the ramps in association with growing thrust anticlines (A1 to A5, Fig. 3b and 11).

7. Discussion

7.1. Channel erosion and implications to the evolution of the Nankai accretionary wedge

The data in this paper show that Quaternary deformation seaward of the MSF is recorded ubiquitously in the form of uplifted pop-up structures and anticlines, as those adjacent to the S1 and S2 thrust faults (A2 and A4; Fig. 3b, 4 and 5). Most of this deformation occurred during the deposition of Unit Ic. However, the evidence in this paper shows that a significant part of movement in thrusted sequences is at present, and was after 1.67 Ma, accommodated by strata in the slope basin. This resulted in the generation of low-amplitude folds, local thrusts, normal faults and complex thrust-fault splays crossing the younger strata in Unit I, particularly in the region adjacent to the S1 and S2 thrusts (Figs. 2, 4 and 5). Major periods of deformation occurring after 1.67 Ma in the accretionary wedge are consequently revealed by enhanced erosion, faulting and deposition of MTDs around active structures (e.g. Strasser et al., 2009; Kimura et al., 2011).

Offshore Nankai, the activity of the MSF has been considered as a main controlling factor on the geometry of the Kumano Basin and adjacent imbricate thrust zone (Moore et al., 2007; Strasser et al., 2009). In particular, the MSF was interpreted to reflect distinct stages of activity in the Quaternary and progressive landward branching of the shallowmost fault segments since ~1.24–1.0 Ma (Moore et al., 2007; Kimura et al., 2011). A different approach to previous work is that of considering erosion as a trigger of deformation within the accretionary prism. In fact, sub-critical conditions in thrust belts require internal (contractional) deformation in order to build taper prior to their forward advance (e.g. Davis et al., 1983; Morley, 2009). Knowing this, we postulate that increasing rates of surface denudation related to channel erosion from <1.67 to 1.24 Ma triggered subcritical conditions on the Nankai continental slope, later leading to important deformation of the upper part of the Nankai slope and the triggering of MTD 6. This postulate contrasts with the understanding that super-critical conditions are commonly recorded upslope from the toe of accretionary wedges due to thicker sedimentary overburdens and fluctuations in basal friction (Davis et al., 1983).

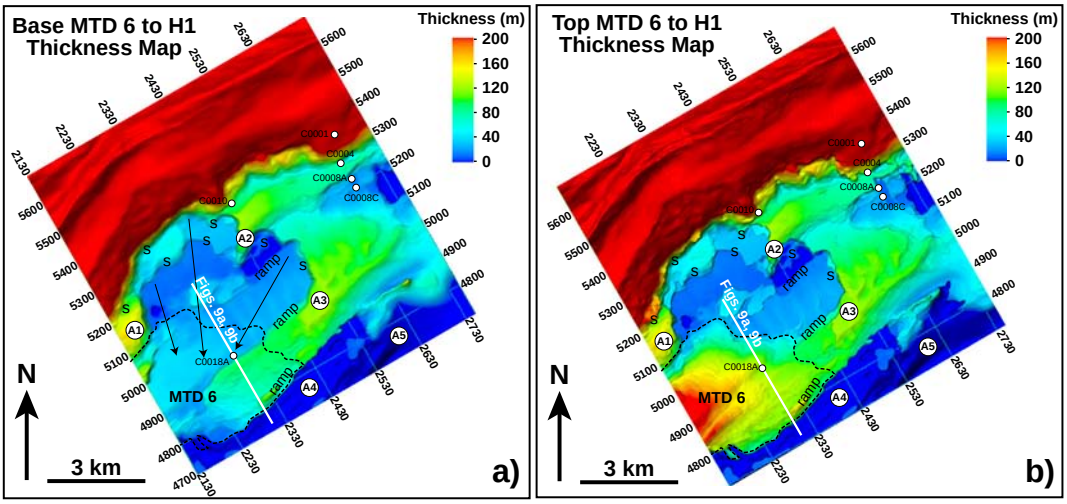

Fig. 10. Structural and thickness maps for key horizons bounding MTD 6. (a) Thickness map of strata between the basal glide plane of MTD 6 (horizon B) and horizon H1, highlighting the series of scarps and frontal ramps referred to in the text. Translation vectors for MTD6 are shown based on the geometry of the main headwall cusps. (b) Thickness map between the top of MTD 6 (horizon A) and horizon H1 highlighting the lateral extent and thickness of MTD 6.

Please cite this article as: Alves, T.M., et al., Erosional features as indicators of thrust fault activity (Nankai Trough, Japan), Marine Geology (2013), http://dx.doi.org/10.1016/j.margeo.2013.07.011

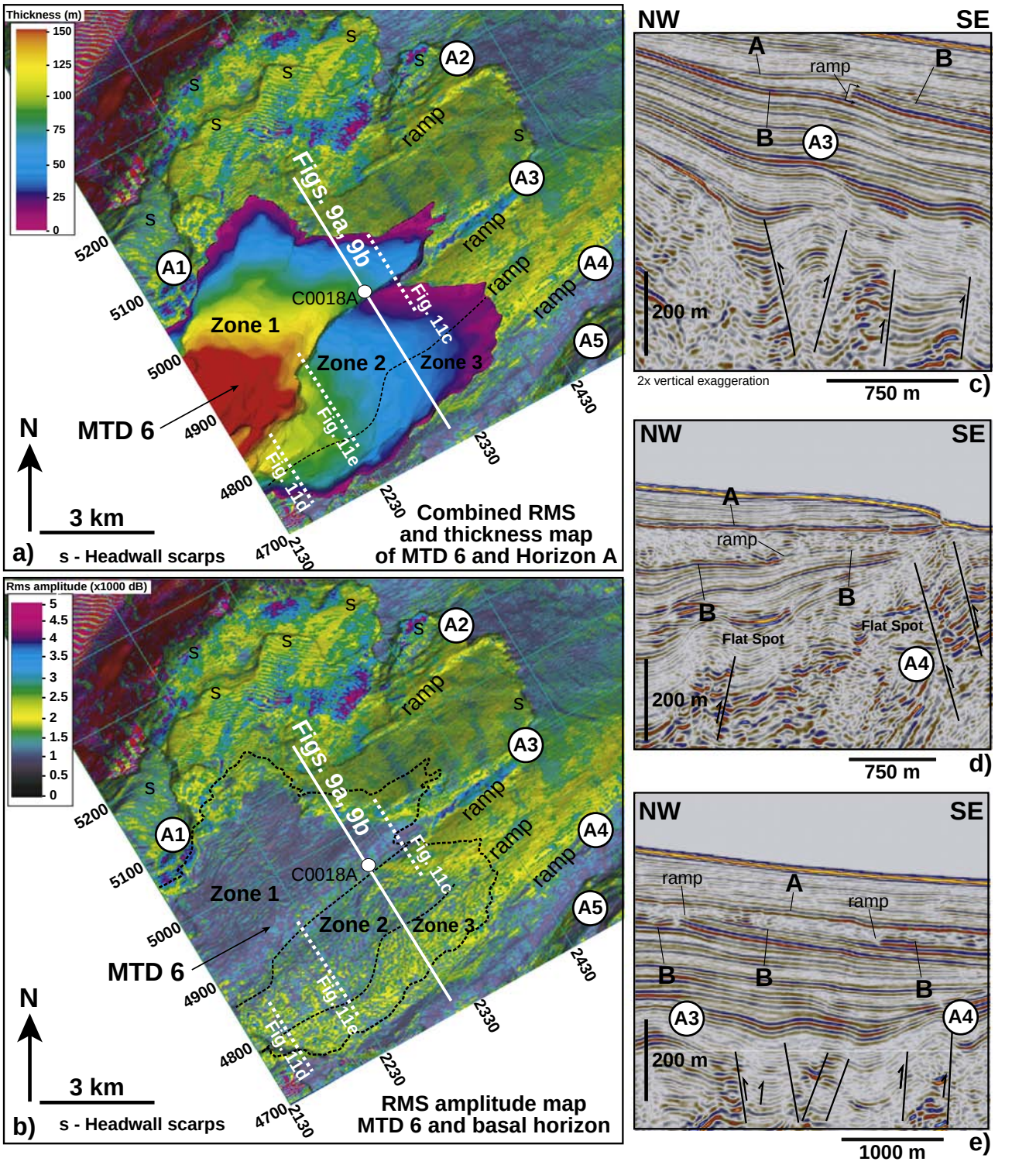

Fig. 11. a) Combined RMS amplitude and thickness map highlighting the position of ramps and resulting thickness variations in MTD 6. b) RMS amplitude map of MTD 6 and underlying basal glide surface. Note the presence of three distinct zones in MTD 6 in terms of its amplitude distribution. Ramps in the figure mark the boundaries between distinct amplitude zones in the MTD. c) Detail of seismic inline 2343 showing the geometry of basal ramps above A3. Throughout the study area, a marked basal ramp was formed above the A3 anticline in response to MTD 6 downslope translation. d) Seismic inline 2193 showing the geometry of basal ramps adjacently to the A4 thrust anticline. e) Seismic inline 2297 showing two basal ramps in the distal part of MTD 6. The ramp to the right was formed at the northern flank of A4, in a broader monocline region.

Our observations have the following implications: significant episodes of seafloor erosion, particularly resulting from features of the scale of the axial channel observed in the study area, can generate periods of more intense thrust-wedge deformation. As a result, these intense periods of erosion need to be recognised on seismic data prior to estimating their magnitudes and spatial distribution by mathematical and physical models, which are commonly based on the present-day taper geometry. As some of these models recognise erosion as a way to produce sub-critical wedges (e.g. Graveleau and Dominguez, 2008; Konstantinovskaya and Malavieille, 2011), it is paramount to ground-truth them with evidence for enhanced activity of accretionary wedges.

Please cite this article as: Alves, T.M., et al., Erosional features as indicators of thrust fault activity (Nankai Trough, Japan), Marine Geology (2013), http://dx.doi.org/10.1016/j.margeo.2013.07.011

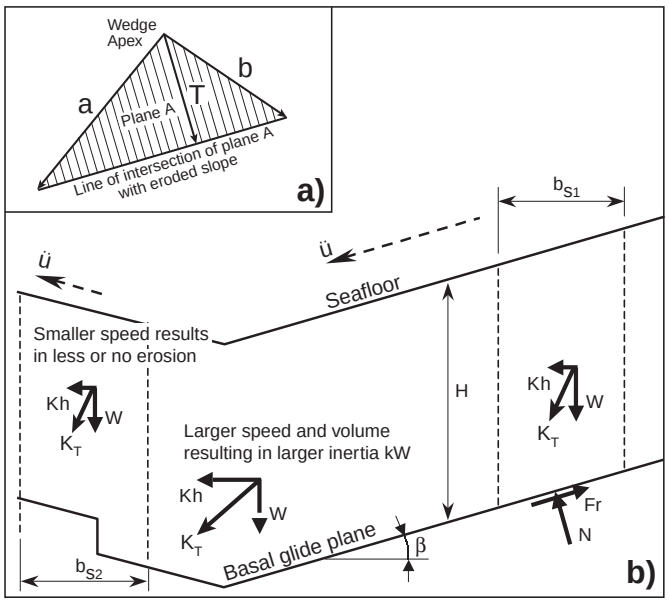

Fig. 12. (a) Diagram highlighting the geometry of orthogonal failure on a slope and the relative angles between side scarps and the resulting transport direction T (from Lucas, 1980). (b) Physical parameters involved in the downslope movement of a block (from Trandafir et al., 2003). Parameters in the figure are described in the text and as Appendix I.

In the specific case of Nankai, a feedback loop between erosion, critical wedge conditions, and tectonic deformation in the MSF may have contributed to larger seafloor deformation rates and, ultimately, to the large-scale slope instability materialised by MTD 6. A consequence of this feedback loop is that the thrust fault activity observed in this paper represents a period of complex, but significant, crustal shortening affecting the upper part of the ITZ after ~1.67 Ma. This conclusion is further highlighted by the distinct thicknesses of strata adjacent to thrust anticlines, favouring a model of diffuse shortening across the Nankai accretionary wedge, and not only landward or adjacently to the MSF.

7.2. Basal ramps of MTDs as indicators of an actively deforming seafloor

In addition to the recognition of submarine channels as proxies for tectonic activity in the ITZ, this paper demonstrates that oblique basal ramps were generated in distal parts of MTD 6 over buried thrust anticlines. Evidence in this work shows that basal ramps were formed when the principal orientations (direction and angle) of seafloor strata changed, a character resulting in variations in the shearing properties of material in the glide plane along the proximal, translation and accumulation regions of MTD 6 (Figs. 11 and 12). Examples of the relationship between the position of basal ramps and underlying thrust anticlines are given in Fig. 11. In the figure, details of basal ramps formed above A2 to A5 are shown; these same ramps occurring at the crest of underlying low-angle anticlines. The most prominent basal ramps (exceeding 45 m in height) are observed above A3 and A4 (Fig. 11). All observed basal ramps are sub-parallel to A1 to A5.

The relationship between buried anticlines and the position of MTD 6 basal ramps can be explained by considering that the horizontal acceleration of a mass-transport body (or slab when moving in a downslope direction) will induce a horizontal inertial force on the glide plane. This way, the movement of a mass-transport body approaches that of a sliding block on a tilted slope (see Newmark, 1965). When a critical angle is reached, shearing (and erosion) adjacent to the glide plane is enhanced above active thrust anticlines (Fig. 12). In these conditions, forces acting on the slope when the movement of a shallow slide, as represented in Fig. 12b, will trigger seafloor failure when the factor of safety (FS) <1 in the following equation:

$$FS = R_s/D_s = \frac{c + (W\ \cos\ \beta - u)\tan\ \phi}{W\ \sin\ \beta}. \quad (1)$$

In Eq. (1), R_s and D_s comprise the sum of all resisting and driving forces, respectively, β is the inclination angle of the glide plane, W is the unit weight at a given point in the slide, c is the effective cohesion of the material, ϕ the internal friction angle and u is water pressure at the base of the slide. The equation is valid for unit areas at the base tending to zero (L −>0; see also Appendix I).

Eq. (1) is valid for a static analysis of slope stability. However, the presence of thrust-parallel scarps at the base of MTD 6 suggests that the horizontal acceleration of the moving mass transport-body (or moving slabs) induces a horizontal inertial force on the glide plane, $k_h(t)W$, not considered in Eq. (1). As a result, variations in the horizontal inertial force of moving mass-transport bodies over active (i.e. seafloor-deforming) thrust anticlines can generate basal scarps and ramps. This same inertial force will relate to unit weight above the glide plane, and to any changes in the slope angle β. The magnitudes of the inertial force will vary in time and space according to slope roughness and the physical properties of moving mass-transport body (Fig. 12b).

This paper proposes that a vector sum of horizontal (and vertical) inertial forces $k_T(t)W$ should replace the parameter 'static weight' (W) at any given point of the basal glide plane, to give us a sum of inertial forces P. This means that with changing slope angles (β) resulting from underlying active thrusts, or any other tectonic features affecting seafloor topography, the basic assumption of Eq. (1) (i.e. infinite slope model with L − >0) is not justified. Instead, at any given point in a not-infinite-slope-model, with changing slope angle, we need to consider the inertial forces and use the vector sum to replace the 'static weight' W such as:

$$P = \sum kT(t)_i \gamma Hb_i = kT(t)_1 \gamma Hb_1 + kT(t)_2 \gamma Hb_2 + \ldots + kT(t)_n \gamma Hb_n \quad (2)$$

in which material inertia kT is a vectorial property varying in the three dimensions and in time such as it approaches variations in a tensor field:

$$k_T(t) = a_x I + a_y J + a_z K. \quad (3)$$

In Eq. (3), I, J and K represent tensor magnitudes in the Cartesian space. The existence of this spatially variable inertial force is our favoured explanation for the generation of oblique ramps underneath the MTDs in the study area. Thus, rather than solely comprising kinematic indicators, scarps and ramps at the base of MTDs can record: a) topographic variations related to structures deforming the seafloor at the time of slope failure, b) regions where shear strength of seafloor sediments varies significantly, and c) abrupt variations in material inertia when of slope failure. Whilst a) proves the utility of MTDs to the recognition (and thus relative dating) of tectonically-active structures, b) and c) suggest scarps and ramps to form boundaries between zones in MTDs with distinct petrophysical properties, as suggested by RMS amplitude data from strata in MTD 6 (Fig. 11).

8. Conclusions

We searched for evidence for late Quaternary movements in the imbricate thrust zone (ITZ) of the Nankai Trough accretionary complex. Seafloor deformation during the Quaternary is mainly recorded in the form of pop-up structures to the south of the study area. In addition, there is evidence on seismic data that a significant part of seafloor deformation in the study area has been accommodated by splays of the larger MSF.

Please cite this article as: Alves, T.M., et al., Erosional features as indicators of thrust fault activity (Nankai Trough, Japan), Marine Geology (2013), http://dx.doi.org/10.1016/j.margeo.2013.07.011

We demonstrate that the incision of submarine channels and gullies occurred in association with significant deformation of the Imbricate Thrust Zone (ITZ) some 300 ky prior to an interpreted phase of forearc uplift and landward tilting, which isolated the Kumano Basin from the Nankai Trough (e.g. Gulick et al., 2010). Later between ~1.05 and 0.85 Ma, MTD 6 was generated and large slabs of strata were eroded on top of active tectonic structures. In addition, it is shown that:

a) The morphology and relative location of submarine gullies, scarps and ramps can be used as proxies to identify active tectonic structures with seafloor expression;
b) Basal ramps can be associated with zones in MTDs with distinct geological properties, but not always comprise reliable kinematic indicators as their generation relates to the combined effect of the mass-transport body erosional power and any pre-existing seafloor roughness;
c) Submarine gullies can be associated with periods of enhanced wedge deformation — imposing subcritical conditions on a part of the slope usually dominated by supercritical conditions.

A corollary of this work is that the relative quiescence in activity recorded by the MSF between ~1.8 and ~1.55 Ma (Strasser et al., 2009) is shown to be accompanied by significant deformation of the accretionary wedge between <1.67 and 0.85 Ma, namely through progressive faulting and activity in thrust faults in the ITZ. Thus together with enhanced activity in the MSF, seafloor deformation in the younger part of the ITZ must be taken in consideration in any evolutionary model for the Nankai Trough.

Acknowledgements

This research used samples and data provided by the Integrated Ocean Drilling Program (IODP). Schlumberger provided the Petrel® software package used to interpret the seismic data in this work. We thank M. Huuse, L. Moscardelli and two anonymous reviewers for their comments. This work was supported by the Swiss National Science Foundation (grant 133481 to M.S.).

Appendix I. Parameters used in equations and Fig. 12 and in the text include

a and b	maximum slope gradients at the margins of the failed slab
b_s	basal surface area of a slide, or slab
c	effective cohesion
$k_h(t)$	horizontal inertia of a slide, slab, or MTD
k_T	material inertia vector
g	gravity force
u	water pressure at the base of a slide, or slab
ü	acceleration tensor of a slide, slab, or MTD
D_s	static driving force imposed on a moving slab
Fr	Friction between the base of a slab and the sliding surface
FS	Safety Factor
H	Height of MTD strata above the glide plane
T	transporting direction of a downslope-moving slab
R_s	available resisting force at the base of a moving slab
W	unit weight at a given point of a slide, or slab
β	slope angle
γ	submersed density
ϕ	internal friction angle of material in the MTD

References

Ashabranner, L.B., Tripsanas, E.K., Shipp, R.C., 2010. Multi-direction flow in a mass-transport deposit, Santos Basin, Offshore Brazil. Advances in Natural and Technological Hazards Research 28, 247–255.

Ashi, J., Taira, A., 1992. Structure of the Nankai accretionary prism as revealed from IZANAGI sidescan imagery and multichannel seismic reflection profiling. Island Arc 1, 104–115.

Bangs, N.L., Cande, S.C., 1997. Episodic development of a convergent margin inferred from structures and processes along the southern Chile margin. Tectonics 16, 489–503. http://dx.doi.org/10.1016/S0040-1951(02)00399-2.

Bangs, N.L.B., Moore, G.F., Gulick, S.P.S., Pangborn, E.M., Tobin, H.J., Kuramoto, S., Taira, A., 2009. Broad, weak regions of the Nankai Megathrust and implications for shallow coseismic slip. Earth and Planetary Science Letters 284, 44–49.

Beaumont, C., Ellis, S., Pfiffner, A., 1999. Dynamics of sediment subduction–accretion at convergent margins: Short-term modes, long-term deformation, and tectonic implications. Journal of Geophysical Research 104 (B8), 17573. http://dx.doi.org/10.1029/1999JB900136.

Berger, P., Johnson, A.M., 1980. First-order analysis of deformation of a thrust sheet moving over a ramp. Tectonophysics 70, T9–T24.

Brown, A.R., 1999. Interpretation of three-dimensional seismic data: American Association of Petroleum Geologists. Memoir 9 (514 pp.).

Buiter, S., 2012. A review of brittle compressional wedge models. Tectonophysics 530-531, 1–17. http://dx.doi.org/10.1016/j.tecto.2011.12.018.

Bull, S., Cartwright, J., Huuse, M., 2009. A review of kinematic indicators from mass-transport complexes using 3D seismic data. Marine and Petroleum Geology 26, 1132–1151.

Byrne, T.B., Lin, W., Tsutsumi, A., Yamamoto, Y., Lewis, J.C., Kanagawa, K., Kitamura, Y., Yamagushi, A., Kimura, G., 2009. Anelastic strain recovery reveals extension across SW Japan subduction zone. Geophysical Research Letters 36, L23310. http://dx.doi.org/10.1029/2009GL040749.

Camerlenghi, A., Pini, G.A., 2009. Mud volcanoes, olistostromes and Argille scagliose in the Mediterranean region. Sedimentology 56, 319–365. http://dx.doi.org/10.1111/j.1365-3091.2008.01016.x.

Covault, J., Fildani, A., Romans, B.W., MacHargue, T., 2011. The natural range of submarine canyon-and-channel longitudinal profiles. Geosphere 7, 313–332.

Dahlen, F.A., 1984. Mechanics of fold-and-thrust belts and accretionary wedges: cohesive Coulomb theory. Journal of Geophysical Research 89, 10087–10101.

Dahlen, F.A., 1990. Critical taper model of fold-and-thrust belts and accretionary wedges. Annual Reviews of Earth and Planetary Sciences 18, 55–99.

Davis, D., Suppe, J., Dahlen, F.A., 1983. Mechanics of fold-and-thrust belts and accretionary wedges. Journal of Geophysical Research 88, 1153–1172.

Dominguez, S., Lallemand, S.E., Malavieille, J., von Huene, R., 1998. Upper plate deformation associated with seamount subduction. Tectonophysics 293, 207–224.

Dominguez, S., Malavieille, J., Lallemand, S.E., 2000. Deformation of accretionary wedges in response to seamount subduction — insights from sandbox experiments. Tectonics 19, 182–196.

Expedition 314 Scientists, 2009. Expedition 314 Site C0004. NanTroSEIZE Stage 1: Investigations of Seismogenesis, Nankai Trough, Japan: Proceedings of the Integrated Ocean Drilling Program 314/315/316. http://dx.doi.org/10.2204/iodp.proc.314315316.116.2009.

Expedition 316 Scientists, 2009a. Expedition 316 Site C0008. NanTroSEIZE Stage 1: Investigations of Seismogenesis, Nankai Trough, Japan: Proceedings of the Integrated Ocean Drilling Program 314/315/316. http://dx.doi.org/10.2204/iodp.proc.314315316.136.2009.

Expedition 316 Scientists, 2009b. Expedition 316 Site C0004. NanTroSEIZE Stage 1: Investigations of Seismogenesis, Nankai Trough, Japan: Proceedings of the Integrated Ocean Drilling Program 314/315/316. http://dx.doi.org/10.2204/iodp.proc.314315316.133.2009.

Expedition 333 Scientists, 2011. NanTroSEIZE Stage 2: subduction inputs 2 and heat flow. IODP Preliminary Reports 333. http://dx.doi.org/10.2204/iodp.pr.333.2011.

Finnegan, N.J., Roe, G., Montgomery, D.R., Hallet, B., 2005. Controls on the channel width of rivers: implications for modelling fluvial incision of bedrock. Geology 33, 229–232.

Gee, M.J.R., Gawthorpe, R.L., Friedmann, J.S., 2005. Giant striations at the base of a submarine landslide. Marine Geology 214, 287–294.

Graveleau, F., Dominguez, S., 2008. Analogue modelling of the interaction between tectonics, erosion and sedimentation in foreland thrust belts. Comptes Rendus Geosciences 340, 324–333.

Gulick, S.P.S., Bangs, N.L.B., Moore, G.F., Ashi, J., Martin, K.M., Sawyer, D.S., Tobin, H.J., Kuramoto, S., Taira, A., 2010. Rapid forearc basin uplift and megasplay fault development from 3D seismic images of Nankai Margin off Kii Peninsula, Japan. Earth and Planetary Science Letters 300, 55–62.

Hampton, M.A., Lee, H., Locat, J., 1996. Submarine landlsides. Reviews of Geophysics 34, 33–59.

Hancock, P.L., 1985. Brittle microtectonics: principles and practice. Journal of Structural Geology 7, 437–457.

Heiniö, P., Davies, R., 2007. Knickpoint migration in submarine channels in response to fold growth, western Niger Delta. Marine and Petroleum Geology 24, 434–449.

Humphrey, N.F., Konrad, S.K., 2000. River incision or diversion in response to bedrock uplift. Geology 28, 43–46.

Huyghe, P., Foata, M., Deville, E., Mascle, G., Caramba Working Group, 2004. Channel profiles through the active thrust front of the southern Barbados prism. Geology 32, 429–432.

Ikari, M.J., Strasser, M., Saffer, D.M., Kopf, A.J., 2011. Submarine landslide potential near the megasplay fault at the Nankai subduction zone. Earth and Planetary Science Letters 312, 453–462. http://dx.doi.org/10.1016/j.epsl.2011.10.024.

Ike, T., Moore, G.F., Kuramoto, S., Park, J.O., Kaneda, Y., Taira, A., 2008. Variations in sediment thickness and type along the northern Philippine Sea plate at the Nankai Trough. Island Arc 17, 342–357. http://dx.doi.org/10.1111/j.1440-1738.2008.00624.x.

Kagohara, K., Ishiyama, T., Imaizumi, T., Miyauchi, T., Sato, H., Matsuta, N., Miwa, A., Ikawa, T., 2009. Subsurface geometry and structural evolution of the eastern margin fault zone of the Yokote basin based on seismic reflection data, northeast Japan. Tectonophysics 470, 319–328.

Kimura, G., Moore, G.F., Strasser, M., Screaton, E., Curewitz, D., Streiff, C., Tobin, H., 2011. Spatial and temporal evolution of the megasplay fault in the Nankai

Please cite this article as: Alves, T.M., et al., Erosional features as indicators of thrust fault activity (Nankai Trough, Japan), Marine Geology (2013), http://dx.doi.org/10.1016/j.margeo.2013.07.011

Trough. Geochemistry, Geophysics, Geosystems 12, Q0A008. http://dx.doi.org/10.1029/2010GC003335.
Kinoshita, M., Tobin, H., Ashi, J., Kimura, G., Lallemant, S., Screaton, E.J., Curewitz, D., Masago, H., Moe, K.T., the Expedition 314/315/316 Scientists, 2009. NanTroSEIZE Stage 1: Investigations of Seismogenesis, Nankai Trough, Japan. Proceedings of the Integrated Ocean Drilling Program 314/315/316. http://dx.doi.org/10.2204/iodp.proc.314315316.2009.
Kitamura, Y., Yamamoto, Y., 2012. Records of submarine landslides in subduction input recovered by IODP Expedition 322, Nankai Trough, Japan: submarine mass movements and their consequences. Advances in Natural and Technological Hazards Research 31, 659–670.
Kolla, V., 2007. A review of sinuous channel avulsion patterns in some major deep-sea fans and factors controlling them. Marine and Petroleum Geology 24, 450–469.
Konstantinovskaya, E.A., Malavieille, J., 2005. Accretionary orogens: erosion and exhumation. Geotectonics 39, 69–86.
Konstantinovskaya, E.A., Malavieille, J., 2011. Thrust wedges with décollement levels and syntectonic erosion: a view from analog models. Tectonophysics 502, 336–350.
Korup, O., Clague, J.J., Hermanns, R.L., Hewitt, K., Strom, A.L., Weidinger, J.T., 2007. Giant landslides, topography, and erosion. Earth and Planetary Science Letters 261, 578–589.
Lague, D., Crave, A., Davy, P., 2003. Laboratory experiments simulating the geomorphic response to tectonic uplift. Journal of Geophysical Research 108. http://dx.doi.org/10.1029/2002JB001785.
Lavé, J., Avouac, J.P., 2011. Fluvial incision and tectonic uplift across the Himalayas of central Nepal. Journal of Geophysical Research 106, 26561–26591.
Lewis, K.B., Carter, L., Davey, F.J., 1994. The opening of Cook Strait: interglacial tidal scour and aligning basins at a subduction to transform plate edge. Marine Geology 116, 293–312. http://dx.doi.org/10.1016/0025-3227(94)90047-7.
Lin, W., Doan, M.-L., Moore, J.C., McNeill, L., Ito, T.T., Saffer, D., Kinoshita, M., Sanada, Y., Moe, K.T., Araki, E., Tobin, H., Kano, Y., et al., 2010. Present-day principal horizontal stress orientations in the Kumano forearc basin of the southwest Japan subduction zone determined from IODP NanTroSEIZE drilling site C0009. Geophysical Research Letters 37, L13303. http://dx.doi.org/10.1029/2010GL043158.
Lucas, J.M., 1980. A general stereographic method for determining the possible mode of failure of any tetrahedral rock wedge. International Journal of Rock Mechanics, Mineral Sciences and Geomechanics 17, 57–61.
Lucente, C.C., Pini, G.A., 2008. Basin-wide mass-wasting complexes as markers of the Oligo-Miocene foredeep-accretionary wedge evolution in the Northern Apennines, Italy. Basin Research 20, 49–71.
Mann, P., Taylor, F.W., Lagoe, M.B., Quarles, A., Burr, G., 1998. Accelerating late Quaternary uplift of the New Georgia Island Group (Solomon island arc) in response to subduction of the recently active Woodlark spreading center and Coleman seamount. Tectonophysics 295, 259–306.
Maruyama, T., Lin, A., 2000. Tectonic history of the Rokko active fault zone (southwest Japan) as inferred from cumulative offsets of stream channels and basement rocks. Tectonophysics 323, 197–216.
Masek, J.G., Isacks, B.L., Gubbels, T.L., Fielding, E.J., 1994. Erosion and tectonics at the margins of continental plateaus. Journal of Geophysical Research 99, 13941–13956.
Matsushi, Y., Wasaka, S., Matsuzaki, H., Matsukuka, Y., 2006. Long-term denudation rates of actively uplifting hillcrests in the Boso Peninsula, Japan, estimated from depth profiling of in situ-produced cosmogenic ^{10}Be and ^{26}Al. Geomorphology 82, 283–294.
Micallef, A., Mountjoy, J.J., 2011. A topographic signature of a hydrodynamic origin for submarine gullies. Geology 39, 115–118.
Mitchell, N.C., 2005. Interpreting long-profiles of canyons in the USA Atlantic continental slope. Marine Geology 214, 75–99. http://dx.doi.org/10.1016/j.margeo.2004.09.005.
Moore, G.F., Bangs, N.L., Taira, A., Kuramoto, S., Pangborn, E., Tobin, H.J., 2007. Three-dimensional splay fault geometry and implications for tsunami generation. Science 318, 1128.
Moore, G.F., et al., 2009. Structural and seismic stratigraphic framework of the NanTroSEIZE State 1 transect. NanTroSEIZE Stage 1: Investigations of Seismogenesis, Nankai Trough, Japan: Proceedings Integrated Ocean Drilling Program 314/315/316. http://dx.doi.org/10.2204/iodp.proc.314315316.102.2009.
Morley, C., 2009. Growth of folds in a deep-water setting. Geosphere 5, 59–89. http://dx.doi.org/10.1130/GES00186.1.
Moscardelli, L., Wood, L., 2008. New classification system for mass transport complexes in offshore Trinidad. Basin Research 20, 73–98.
Mountjoy, J.J., Barnes, P.M., Pettinga, J.R., 2009. Morphostructure and evolution of submarine canyons across an active margin: Cook Strait sector of the Hikurangi Margin, New Zealand. Marine Geology 260, 45–68. http://dx.doi.org/10.1016/j.margeo.2009.01.006.
Nakada, M., Tahara, M., Shimizu, H., Nagaoka, S., Uehira, K., Suzuki, S., 2002. Late Pleistocene crustal uplift and gravity anomaly in the eastern part of Kyushu, Japan, and its geophysical implications. Tectonophysics 351, 263–283.
Nemec, W., 1990. Aspects of sediment movement on steep delta slopes. In: Colella, A., Prior, D.B. (Eds.), Coarse-grained deltas. International Association of Sedimentology Special Publication, 10, pp. 29–73.
Newmark, N., 1965. Effects of earthquakes on dams and embankments. Geotechnique 15, 139–160.
Orange, D.L., 1999. Tectonics, sedimentation, and erosion in northern California: submarine geomorphology and sediment preservation potential as a result of three competing processes. Marine Geology 154, 369–382.
Park, J.-O., Tsuru, T., Kodaira, S., Cummins, P.R., Kaneda, Y., 2002. Splay fault branching along the Nankai subduction zone. Science 297, 1157–1160.
Pratson, L.F., Coakley, B.J., 1996. A model for the headward erosion of submarine canyons induced by downslope-eroding sediment flows. Bulletin of the Geological Society of America 108, 225–234.
Pratson, L.F., Ryan, W.B.F., Mountain, G.S., Twichell, D.C., 1994. Submarine canyon initiation by downslope-eroding sediment flows: evidence in late Cenozoic strata on the New Jersey continental slope. Bulletin of the Geological Society of America 106, 395–412.
Ratzov, G., Sosson, M., Collot, J.-Y., Migeon, S., 2012. Late Quaternary geomorphologic evolution of submarine canyons as a marker of active deformation on convergent margins: the example of the South Colombian margin. Marine Geology 315–318, 77–97.
Sakagushi, A., Kimura, G., Strasser, M., Screaton, E.J., Curewitz, D., Murayama, M., 2011. Episodic seafloor mud brecciation due to great subduction zone earthquakes. Geology 39, 919–922.
Sibson, R.H., 1998. Brittle failure mode plots for compressional and extensional tectonic regimes. Journal of Structural Geology 20, 655–660.
Smit, J., Burg, J.P., Dolati, A., Solutis, D., 2010. Effects of mass waste events on thrust wedges: analogue experiments and application to the Makran accretionary wedge. Tectonics 29, TC3003. http://dx.doi.org/10.1029/2009TC002526.
Strasser, M., Moore, G., Kimura, G., Kitamira, Y., Kopf, A.J., Lallemant, S., Park, J.-O., Screaton, E., Su, X., Underwood, M.B., Zhao, X., 2009. Origin and evolution of a splay fault in the Nankai accretionary wedge. Nature Geoscience 2, 648–652.
Strasser, M., Moore, G.F., Kimura, G., Kopf, A.J., Underwood, M.B., Guo, J., Screaton, E.J., 2011. Slumping and mass transport deposition in the Nankai fore arc: evidence from IODP drilling and 3-D reflection seismic data. Geochemistry, Geophysics, Geosystems 12, Q0AD13. http://dx.doi.org/10.1029/2010GC003431.
Strasser, M., Henry, P., Kanamatsu, T., Thu, M.K., Moore, G.F., the IODP Expedition 333 Scientists, 2012. Scientific drilling of mass-transport deposits in the Nankai accretionary wedge: first results from IODP Expedition 333. In: Yamada, Y., et al. (Ed.), Submarine Mass Movements and Their Consequences. Advances in Natural and Technological Hazard Research, 31, pp. 671–681. http://dx.doi.org/10.1007/978-94-007-2162-3_60.
Tamaki, M., Kusumoto, S., Itoh, Y., 2009. Formation and deformation processes of late Paleogene sedimentary basins in southern central Hokkaido, Japan: paleomagnetic and numerical modeling approach. Island Arc 19, 243–258.
Tobin, H.J., Kinoshita, M., 2006. NanTroSEIZE: the IODP Nankai trough seismogenic zone experiment. Scientific Drilling 2, 23–27.
Trandafir, A.C., Sassa, K., Fukuoka, H., 2003. Assessment of Undrained Seismic Displacement on Shear Surfaces in Saturated Cohesionless Soils. Annuals of Disaster Prevention Research Institute, Kyoto University 46.
Tsuru, T., Park, J.-O., Takahashi, N., Kodaira, S., Kido, Y., Kaneda, Y., Kono, Y., 2000. Tectonic features of the Japan Trench convergent margin off Sanriku, northeastern Japan, revealed by multichannel seismic reflection data. Journal of Geophysical Research 105, B07. http://dx.doi.org/10.1029/2000JB900132.
Turowski, J.M., Lague, D., Crave, A., Hovius, N., 2006. Experimental channel response to tectonic uplift. Journal of Geophysical Research 111, F03008. http://dx.doi.org/10.1029/2005JF000306.
Turowski, J.M., Hovius, N., Meng-Long, H., Lague, D., Men0Chiang, M., 2008. Distribution of erosion across bedrock channels. Earth Surface Processes and Landforms 33, 353–363.
Turowski, J.M., Lague, D., Hovius, N., 2009. Response of bedrock channel width to tectonic forcing: insights from a numerical model, theoretical considerations, and comparison with field data. Journal of Geophysical Research 114. http://dx.doi.org/10.1029/2008JF001133.
von Huene, R., Ranero, C., Watts, P., 2005. Tsunamigenic slope failure along the Middle America Trench in two tectonic settings. Marine Geology 203, 303–317.
Wang, K., He, J., 1999. Mechanics of low-stress forearcs: Nankai and Cascadia. Journal of Geophysical Research - Solid Earth 104, 15191–15205. http://dx.doi.org/10.1029/1999JB900103.
Wang, K., Hu, Y., 2006. Accretionary prisms in subduction earthquake cycles: the theory of dynamic Coulomb wedge. Journal of Geophysical Research 111, B06410. http://dx.doi.org/10.1029/2005JB004094.
Yamada, Y., Yamashita, Y., Yamamoto, Y., 2010. Submarine landslides at subduction margins: insights from physical models. Tectonophysics 484, 156–167. http://dx.doi.org/10.1016/j.tecto.2009.09.007.
Yamada, Y., Oshima, Y., Matsuoka, T., 2012. Slope failures in analogue models of accretionary wedges. In: Yamada, Y., et al. (Ed.), Submarine Mass Movements and Their Consequences. Advances in Natural and Technological Hazards Research, 31. http://dx.doi.org/10.1007/978-94-007-2162-3_31.

Please cite this article as: Alves, T.M., et al., Erosional features as indicators of thrust fault activity (Nankai Trough, Japan), Marine Geology (2013), http://dx.doi.org/10.1016/j.margeo.2013.07.011